Journal of Quantitative Spectroscopy & Radiative Transfer 112 (2011) 2619–2629

Contents lists available at ScienceDirect

Journal of Quantitative Spectroscopy & Radiative Transfer

journal homepage: www.elsevier.com/locate/jqsrt

# Multiple-scaling methods for Monte Carlo simulations of radiative transfer in cloudy atmosphere

Zhen Wang [a,b,*], Shizhi Yang [a,b], Yanli Qiao [a,b], Shengcheng Cui [a,b], Qiang Zhao [a,b]

[a] Center for Optical Remote Sensing, Anhui Institute of Optics and Fine Mechanics, Chinese Academy of Sciences, Hefei 230031, PR China
[b] Key Laboratory of Optical Calibration and Characterization, Chinese Academy of Sciences, Hefei 230031, PR China

ARTICLE INFO

*Article history:*
Received 29 January 2011
Received in revised form
4 June 2011
Accepted 23 June 2011
Available online 7 July 2011

*Keywords:*
Multiple-scaling
Monte Carlo
Radiative transfer
Cloud field

ABSTRACT

Two multiple-scaling methods for Monte Carlo simulations were derived from integral radiative transfer equation for calculating radiance in cloudy atmosphere accurately and rapidly. The first one is to truncate sharp forward peaks of phase functions for each order of scattering adaptively. The truncated functions for forward peaks are approximated as quadratic functions; only one prescribed parameter is used to set maximum truncation fraction for various phase functions. The second one is to increase extinction coefficients in optically thin regions for each order scattering adaptively, which could enhance the collision chance adaptively in the regions where samples are rare. Several one-dimensional and three-dimensional cloud fields were selected to validate the methods. The numerical results demonstrate that the bias errors were below 0.2% for almost all directions except for glory direction (less than 0.4%) and the higher numerical efficiency could be achieved when quadratic functions were used. The second method could decrease radiance noise to 0.60% for cumulus and accelerate convergence in optically thin regions. In general, the main advantage of the proposed methods is that we could modify the atmospheric optical quantities adaptively for each order of scattering and sample important contribution according to the specific atmospheric conditions.



## 1. Introduction

Rapid and accurate radiative transfer model is essential to evaluate the earth's radiation budget and retrieve atmospheric components from remote sensing observations. A large number of three-dimensional (3D) radiative effects have been examined using improved numerical modeling from satellite observations at continuously improving spatial resolution, such as the scale break of radiative fields [1], roughening and smoothening of radiative fields [2,3] as well as enhanced clear sky reflectance near clouds [4–7], etc. 3D radiative transfer models as the only tools to examine these effects now become more and more important. Monte Carlo methods as an effective and flexible means are often employed in simulating radiance in cloudy atmosphere realistically. But there are some obstacles in practical applications, such as an inherent slow rate of convergence and very expensive computation taxing for current computational power [8–12]. Partly removing these obstacles is the aim of this study.

Among a variety of variance reduction techniques with biases, the most efficient one may be truncation approximation, which truncates sharp peaks of phase functions for large water or ice droplets at visible wavelength and approximates it to a linear mixture of the delta function and smoothing (regular) function [10,11,13–17] and could accelerate convergence greatly. Two issues should be addressed here. First, a suitable smoothing function should be chosen to match original phase function as much as possible. Antyufeev [17]

* Corresponding author at: Center for Optical Remote Sensing, Anhui Institute of Optics and Fine Mechanics, Chinese Academy of Sciences, Hefei 230031, PR China.
*E-mail address:* intersharp@126.com (Z. Wang).

0022-4073/$ - see front matter © 2011 Elsevier Ltd. All rights reserved.
doi:10.1016/j.jqsrt.2011.06.019

truncated forward peaks directly, which could decrease random noise greatly but introduce large biases; Iwabuchi [11] truncated forward and backward peaks simultaneously with a constraint of conservation for first two moments, which could greatly improve accuracy except in direction near the solar and anti-solar points; Iwabuchi and Suzuki [10] made slightly improvement to replace forward peaks with the flat function, which could have high accuracy in almost all directions at cost of more computation time. The second issue is that how to construct Monte Carlo algorithm to simulate trajectories with different delta fraction dependent on the order scattering. Suzuki et al. [18] and Iwabuchi and Suzuki [10] derived radiative transfer equation (RTE) with scattering order-dependent truncation approximations based on the method of successive orders of scattering (SOS) for 1D and 3D atmosphere, respectively. In this paper, the multiple-scaling methods were derived from integral RTE and could formulate Monte Carlo algorithm and local estimate method directly. The new truncation functions were proposed to replace forward peaks, which were more similar to original phase function than flat functions.

Moreover, the poor sampling in optically thin regions often contaminates estimated radiance, even covers the characterization of radiative fields, such as smoothening of radiative fields and enhanced clear sky reflectance near cloud, which is used to correct 1D retrieval results [19]. All these characterizations are mainly due to multiple scattering. Thus the more high-order scattering we sample in optically thin regions, the more accurate the estimated radiance will be. Iwabuchi [11] proposed collision-forcing method for optically thin media with a domainwide constant (minimum atmospheric optical thickness) to scale optical properties for each atmospheric column. The method may be not economic for partly cloudy atmosphere because it increases collision chances nonuniformly in optically thin regions, too large for column without clouds and too small for column with clouds and at same time it increases simulation time in optically thick regions due to scaled optical thickness. In this paper, we formulate another multiple-scaling method derived from integral RTE, which could scale optical quantities adaptively dependent on the order of scattering. It could be applied to optically thin regions to infer the characterization of radiative fields.

This paper is organized as follows. We make transformation of integral RTE and formulate multiple-scaling methods for anisotropy phase function and optically thin regions based on integral RTE and introduce several truncation approximations in Section 2; the performance of the proposed methods is presented in Section 3; and the last section contains conclusions.

## 2. Multiple-scaling methods

### 2.1. Transformation of integral RTE

The solution of integral RTE in optical medium $\mathbf{R}$ can be represented as a Neumann series [17,20,21]

$$F(\mathbf{r},\mathbf{\Omega}) = \sum_{n=0}^{\infty} F_n(\mathbf{r},\mathbf{\Omega}), \tag{1}$$

where $F(\mathbf{r},\mathbf{\Omega})$ is the collision density in the direction $\mathbf{\Omega}$ at point $\mathbf{r}$, defined as the product of extinction coefficient $\sigma(\mathbf{r})$ and radiance $I(\mathbf{r},\mathbf{\Omega})$, and $F_n(\mathbf{r},\mathbf{\Omega})$ is the collision density of the $n$th order, defined as

$$F_n(\mathbf{r},\mathbf{\Omega}) = \begin{cases} \int_{\mathbf{R}}\int_{\mathbf{\Omega}} k(\mathbf{r}',\mathbf{\Omega}';\mathbf{r},\mathbf{\Omega}) F_{n-1}(\mathbf{r}',\mathbf{\Omega}')\, d\mathbf{\Omega}'\, d\mathbf{r}' & n>0 \\ \sigma \exp(-\sigma\|\mathbf{r}-\mathbf{r}_0\|) & n=0 \end{cases}, \tag{2}$$

where the kernel $k(\mathbf{r}',\mathbf{\Omega}';\mathbf{r},\mathbf{\Omega})$ is the probability density function (PDF) of the transition from phase point $(\mathbf{r}',\mathbf{\Omega}')$ into $(\mathbf{r},\mathbf{\Omega})$ and can be given as

$$k(\mathbf{r}',\mathbf{\Omega}';\mathbf{r},\mathbf{\Omega}) = \omega \frac{P(\mathbf{\Omega}'\cdot\mathbf{\Omega})}{4\pi} \frac{\sigma \exp(-\sigma\|\mathbf{r}-\mathbf{r}'\|)}{\|\mathbf{r}-\mathbf{r}'\|^2} \delta\left(\mathbf{\Omega} - \frac{\mathbf{r}-\mathbf{r}'}{\|\mathbf{r}-\mathbf{r}'\|}\right), \tag{3}$$

where $\omega$ is the single scattering albedo, $P(\mathbf{\Omega}'\cdot\mathbf{\Omega})/4\pi$ is the normalized scattering phase function and $\sigma$ is the extinction coefficient. For simplicity, we assume these quantities to be constants in whole $\mathbf{R}$.

After transformation from the Cartesian to the polar coordinates [17], $F_n(\mathbf{r},\mathbf{\Omega})$ for $n>0$ can be rewritten as

$$F_n(\mathbf{r},\mathbf{\Omega}) = \frac{1}{4\pi}\int_0^{\infty}\int_{\mathbf{\Omega}} \omega P(\mathbf{\Omega}'\cdot\mathbf{\Omega}) f(l) F_{n-1}(\mathbf{r}-l\mathbf{\Omega},\mathbf{\Omega}')\, d\mathbf{\Omega}'\, dl, \quad n>0, \tag{4}$$

where $f(l)$ is free path PDF [22], defined as

$$f(l) = \sigma \exp(-\sigma l). \tag{5}$$

We can let $\mathbf{r}=\mathbf{r}_0+t\mathbf{\Omega}$, $\mathbf{r}'=\mathbf{r}_0+t'\mathbf{\Omega}$ due to $\mathbf{\Omega}=(\mathbf{r}-\mathbf{r}')/\|\mathbf{r}-\mathbf{r}'\|$. Considering that $f(l)=0$ for $l<0$ and changing the variable $l$ to $t$ [17], we can rewrite $F_n(\mathbf{r},\mathbf{\Omega})$ as

$$F_n(t,\mathbf{\Omega}) = \frac{1}{4\pi}\int_{\mathbf{\Omega}} d\mathbf{\Omega}' \omega P(\mathbf{\Omega}'\cdot\mathbf{\Omega}) \int_{-\infty}^{\infty} dt' f(t-t') F_{n-1}(t',\mathbf{\Omega}'), \quad n>0. \tag{6}$$

Here $\int_{-\infty}^{\infty} dt' f(t-t') F_{n-1}(t',\mathbf{\Omega}')$ is the convolution of the functions $f(t)$ and $F_{n-1}(t,\mathbf{\Omega}')$ of a single variable $t$. By applying the Laplace transform with respect to the variable $t$ to both sides of Eq. (6), we obtain

$$\hat{F}_n(s,\mathbf{\Omega}) = \frac{1}{4\pi}\int_{\mathbf{\Omega}} d\mathbf{\Omega}' \omega P(\mathbf{\Omega}'\cdot\mathbf{\Omega}) \hat{f}(s) \hat{F}_{n-1}(s,\mathbf{\Omega}'), \quad n>0, \tag{7}$$

where $\hat{F}_n(s,\mathbf{\Omega})$ and $\hat{f}(s)$ in "$s$-space" are Laplace transform of $F_n(t,\mathbf{\Omega})$ and $f(t)$ in "$t$-space", respectively. According to Eq. (5), $\hat{f}(s)$ could be given as

$$\hat{f}(s) = \frac{\sigma}{s+\sigma}. \tag{8}$$

In addition, $\hat{F}_n(s,\mathbf{\Omega})$ for $n=0$ could be easily formulated as

$$\hat{F}_n(s,\mathbf{\Omega}) = \hat{f}(s), \quad n=0. \tag{9}$$

### 2.2. Multiple-scaling method for anisotropic phase function

In this section, we formulate the multiple-scaling method based on Eqs. (7) and (9), which can construct Monte Carlo algorithms directly for simulating the trajectories of individual sample with different smooth phase functions depending on the order of scattering.

First an approximated phase function $\tilde{P}_n(\mathbf{\Omega}'\cdot\mathbf{\Omega})$ is introduced to replace $P(\mathbf{\Omega}'\cdot\mathbf{\Omega})$, which is a linear mixture of Dirac's delta function and smooth function [10,11,13–17] with different truncation fraction $f_\delta^{(n)}$ for each order independently,

$$\tilde{P}_n(\mathbf{\Omega}'\cdot\mathbf{\Omega}) = f_\delta^{(n)}\delta(\mathbf{\Omega}'-\mathbf{\Omega}) + (1-f_\delta^{(n)})P_n^*(\mathbf{\Omega}'\cdot\mathbf{\Omega}). \tag{10}$$

Substituting Eq. (10) into Eq. (7) instead of $P(\mathbf{\Omega}'\cdot\mathbf{\Omega})$, we obtain

$$\hat{F}_n(s,\mathbf{\Omega}) = \omega f_\delta^{(n)}\hat{f}(s)\hat{F}_{n-1}(s,\mathbf{\Omega}) + \frac{1}{4\pi}\int_{\mathbf{\Omega}} d\mathbf{\Omega}'\omega(1-f_\delta^{(n)})P_n^*(\mathbf{\Omega}'\cdot\mathbf{\Omega})\hat{f}(s)\hat{F}_{n-1}(s,\mathbf{\Omega}'), \quad n>0, \tag{11}$$

then we sum up Eqs. (9) and (11) for all scattering orders

$$\sum_{n=0}^{\infty}\hat{F}_n(s,\mathbf{\Omega}) = \sum_{n=1}^{\infty}\omega f_\delta^{(n)}\hat{f}(s)\hat{F}_{n-1}(s,\mathbf{\Omega}) + \hat{f}(s) + \sum_{n=1}^{\infty}\left[\frac{1}{4\pi}\int_{\mathbf{\Omega}} d\mathbf{\Omega}'\omega(1-f_\delta^{(n)})P_n^*(\mathbf{\Omega}'\cdot\mathbf{\Omega})\hat{f}(s)\hat{F}_{n-1}(s,\mathbf{\Omega}')\right]. \tag{12}$$

Rearranging Eq. (12) for all scattering orders, we obtain

$$\sum_{n=0}^{\infty}\left[(1-\omega f_\delta^{(n+1)}\hat{f}(s))\hat{F}_n(s,\mathbf{\Omega})\right] = \hat{f}(s) + \sum_{n=1}^{\infty}\left[\frac{1}{4\pi}\int_{\mathbf{\Omega}} d\mathbf{\Omega}'\omega(1-f_\delta^{(n)})P_n^*(\mathbf{\Omega}'\cdot\mathbf{\Omega})\hat{f}(s)\hat{F}_{n-1}(s,\mathbf{\Omega}')\right]. \tag{13}$$

Thus a new set of equations for each order can be given as

$$\hat{F}_n(s,\mathbf{\Omega}) = \begin{cases} \dfrac{1}{4\pi}\displaystyle\int_{\mathbf{\Omega}} d\mathbf{\Omega}'\frac{\omega(1-f_\delta^{(n)})}{1-\omega f_\delta^{(n+1)}\hat{f}(s)}P_n^*(\mathbf{\Omega}'\cdot\mathbf{\Omega})\hat{f}(s)\hat{F}_{n-1}(s,\mathbf{\Omega}') & n>0 \\ \dfrac{\hat{f}(s)}{1-\omega f_\delta^{(n+1)}\hat{f}(s)} & n=0 \end{cases}. \tag{14}$$

Next, by applying the inverse Laplace transform to both sides of Eq. (14) and changing the current coordinates to Cartesian coordinates, we obtain

$$F_n^*(\mathbf{r},\mathbf{\Omega}) = \begin{cases} \int_R\int_{\mathbf{\Omega}} k_n^*(\mathbf{r}',\mathbf{\Omega}';\mathbf{r},\mathbf{\Omega})F_{n-1}^*(\mathbf{r}',\mathbf{\Omega}')\,d\mathbf{\Omega}'\,d\mathbf{r}' & n>0 \\ \sigma_{n+1}^*\exp(-\sigma_{n+1}^*\|\mathbf{r}-\mathbf{r}_0\|) & n=0 \end{cases}, \tag{15}$$

where

$$k_n^*(\mathbf{r}',\mathbf{\Omega}';\mathbf{r},\mathbf{\Omega}) = \omega_n^*\frac{P_n^*(\mathbf{\Omega}'\cdot\mathbf{\Omega})}{4\pi}\frac{\sigma_{n+1}^*\exp(-\sigma_{n+1}^*\|\mathbf{r}-\mathbf{r}'\|)}{\|\mathbf{r}-\mathbf{r}'\|^2}\delta\left(\mathbf{\Omega}-\frac{\mathbf{r}-\mathbf{r}'}{\|\mathbf{r}-\mathbf{r}'\|}\right) \tag{16}$$

is a new PDF of the transition scaled by the multiple-scaling method and

$$F_n^*(\mathbf{r},\mathbf{\Omega}) = \sigma_{n+1}^* I_n(\mathbf{r},\mathbf{\Omega}) \tag{17}$$

is the collision density of the $n$th order. The scaled optical quantities for $n$th scattering order can be given by

$$\sigma_{n+1}^* = (1-f_\delta^{(n+1)}\omega)\sigma, \tag{18}$$

$$\omega_n^* = \frac{(1-f_\delta^{(n)})\omega}{1-f_\delta^{(n)}\omega}. \tag{19}$$

Now the collision density

$$F^*(\mathbf{r},\mathbf{\Omega}) = \sum_{n=0}^{\infty}F_n^*(\mathbf{r},\mathbf{\Omega}) \tag{20}$$

gives an approximated solution of integral RTE. The solution compared with its different formalism in [10] could more easily construct Monte Carlo algorithm for simulating samples' trajectories according to the new PDF (see Eq. (16)), which is composed of three PDFs for $n$th order. First we determine whether scattering event occurs according to single scattering PDF $\omega_n^*$ and then select a new direction from scattering direction PDF $P_n^*(\mathbf{\Omega}'\cdot\mathbf{\Omega})/4\pi$, and lastly determine next collision point according to free path PDF $\sigma_{n+1}^*\exp(-\sigma_{n+1}^*\|\mathbf{r}-\mathbf{r}'\|)$. Furthermore, according to the derivation procedures of local estimate method [20,21], the contribution function $\Psi_n^*(\mathbf{r},\mathbf{\Omega})$ of radiance in the direction $\mathbf{\Omega}^*$ at point $\mathbf{r}^*$ for $n$th order could be modified as

$$\Psi_n^*(\mathbf{r},\mathbf{\Omega}) = w_n^*\frac{P_n^*(\mathbf{\Omega}\cdot\mathbf{\Omega}^*)}{4\pi}\frac{\exp(-\sigma_{n+1}^*\|\mathbf{r}^*-\mathbf{r}\|)}{\|\mathbf{r}^*-\mathbf{r}\|^2}\delta_{\mathbf{r}^*,\mathbf{\Omega}^*}(\mathbf{r},\mathbf{\Omega}), \tag{21}$$

where sample's weight is equal to $w_n^* = \prod_{i=1}^n\omega_i^*$. We should note that the extinction coefficient in Eq. (21) should be scaled with respect to $(n+1)$th order when estimating contribution of $n$th order [11]. Although the multiple-scaling method is derived from homogenous optical medium, it could be directly applied to inhomogeneous atmosphere such as partly cloudy atmosphere.

### 2.3. Various truncation approximations for phase function

There are two principles to reasonably represent smooth function $P_n^*(\theta)$ in Eq. (10) (where $\theta$ is hereafter referred to as scattering angle, equal to $\cos^{-1}(\mathbf{\Omega}'\cdot\mathbf{\Omega})$), which is also called as truncated phase function [10,11]. First, a sharp forward peak due to diffraction of cloud drops should be truncated as much as possible, because it can be larger than the minimum phase function by a factor of a million or more at visible wavelengths and thus cause large variance in radiance estimates [9–12]. Second, the similarity between $P(\theta)$ and $P_n^*(\theta)$ at mostly other's direction should be preserved to avoid making huge phase function tables for each different $f_\delta^{(n)}$ [11] and make simulations of multiple scattering radiation field realistically.

In order to fulfill above principles, the truncated phase function can be represented as follows [10]:

$$P_n^*(\theta) = \frac{1}{1-f_\delta^{(n)}}\begin{cases} P_f(\theta) & \theta<\theta_f \\ P(\theta) & \theta\ge\theta_f \end{cases}, \tag{22}$$

where $\theta_f$ is truncated scattering angle. For $\theta\ge\theta_f$, the approximated phase function in Eq. (10) is exactly the same as the original $P(\theta)$. For $\theta<\theta_f$, there are several subjective choices to represent $P_f(\theta)$ [9–11,17]. Here two approximations are introduced as follows:

$$P_f(\theta) = P_F, \tag{23}$$

$$P_f(\theta) = a + b\cos^2\theta. \tag{24}$$

A flat [10] and quadratic function replaces the peak in Eqs. (23) and (24), respectively. The constraint of moment conservation should be added to estimate radiance accurately [11], thus defining the zeroth and first moments of truncation fraction of original and approximated phase function, respectively, as

$$g_{0f} = \frac{1}{2}\int_0^{\theta_f} P(\theta)\sin\theta\, d\theta, \tag{25}$$

$$\hat{g}_{0f} = \frac{1}{2}\int_0^{\theta_f} P_f(\theta)\sin\theta\, d\theta, \tag{26}$$

$$g_{1f} = \frac{1}{2}\int_0^{\theta_f} P(\theta)\cos\theta\sin\theta\, d\theta, \tag{27}$$

$$\hat{g}_{1f} = \frac{1}{2}\int_0^{\theta_f} P_f(\theta)\cos\theta\sin\theta\, d\theta. \tag{28}$$

Due to equalities between two corresponding moments of the original phase function and those of approximated, following equations can be given as:

$$g_{0f} = f_\delta^{(n)} + \hat{g}_{0f}, \tag{29}$$

$$g_{1f} = f_\delta^{(n)} + \hat{g}_{1f}. \tag{30}$$

If $f_\delta^{(n)}$ is a prescribed parameter for flat function approximation, it is flexible to determine the parameters of $\theta_f$ and $P_F$ in Eq. (23) by solving Eqs. (29) and (30), respectively. In order to fulfill second principle, we maintain the continuity of the truncated phase function at truncated scattering angle $\theta_f$ for quadratic function approximation, thus

$$P_f(\theta_f) = P(\theta_f). \tag{31}$$

Therefore we could solve Eqs. (29)–(31) to determine the parameters $\theta_f$, $a$ and $b$ in Eq. (24).

Iwabuchi [11] introduced an efficient method to determine $f_\delta^{(n)}$ according to the statistical directionality parameter $\chi_n$, which could be interpreted as ensemble-averaged cosine angle between initial direction of the sample propagation and the directions for $n$th order [23] and defined as

$$\chi_n = \chi_{n-1}|g_n|, \tag{32}$$

where $g_n$ is the asymmetry factor of the truncated phase function of $n$th order. However the formula of the delta fraction (see Eq. (26) in [11]) was just designed for the truncation approximations in [11], so we slightly modify the formula as

$$f_\delta^{(n+1)} = F_{\max} H(\chi_n), \tag{33}$$

where $H(\chi_n)$ (see Eq. (29) in [11]) is given as

$$H(\chi_n) = \begin{cases} 0 & \chi_n \geq \chi_{\max} \\ h(\chi_n)/h_{\max} & \chi_{\min} \leq \chi_n \leq \chi_{\min} \\ 1 & \chi_n < \chi_{\min} \end{cases} \tag{34}$$

and the maximum delta fraction $F_{\max}$ is a constant for a specific phase function. Following first principle above, the value $P_{\max}$ of phase function as a single tuning parameter is used to determine the maximum truncated scattering angle $\theta_{\max}$ for each phase function, and then $F_{\max}$ is given by

$$F_{\max} = \int_0^{\theta_{\max}} P(\theta)\cos\theta\, d\theta. \tag{35}$$

It diminishes the difficulty of determining $F_{\max}$ for various phase functions. For preliminary tests, $P_{\max}$ could be suited for various phase function from small cloud droplets to large ones.

An example of truncation approximations for phase function of cloud droplet with effective radius 10 μm has been shown in Fig. 1. It shows that quadratic functions were continuous and smooth at truncated scattering angles while flat functions were step functions at these angles. In Table 1, we found that quadratic functions took more truncation fraction $f_\delta^{(n)}$ and they came closer to original phase function for small $H(\chi_n)$ (low order scattering). Thus quadratic functions follow above principles more. In addition, by further analysis, we could know that the parameter $a$ is aimed to truncate forward peaks while the parameter $b$ is used to ensure moment conservation equation (Eqs. (29)

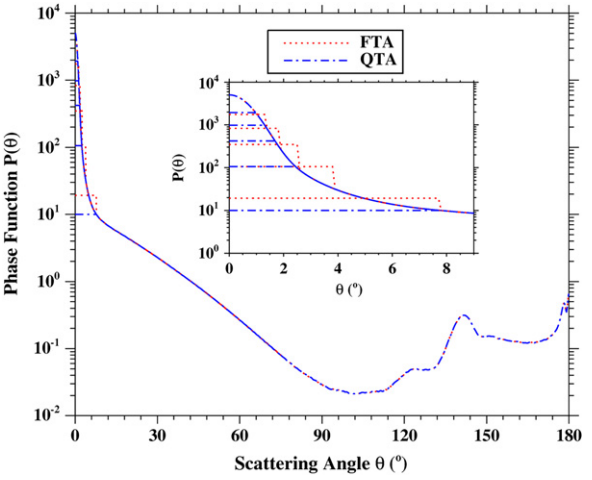


**Fig. 1.** An example of the truncated phase functions with respect to different $H(\chi)$ (see Table 1). Flat (dotted line) and quadratic (dash dot line) functions were used to replace forward peaks. The inset shows the region with a small angle. The tuning parameters were $P_{\max} = 10$ and $h_{\max} = 5$.

**Table 1**
An example of the parameters in the truncated phase functions using both flat and quadratic functions approximation with respect to different $H(\chi_n)$ (see Eq. (34)). The tuning parameters were $P_{\max} = 10$ and $h_{\max} = 5$.

| $H(\chi_n)$ | Flat function approximation | | | Quadratic function approximation | | | |
|---|---|---|---|---|---|---|---|
| | $f_\delta^{(n)}$ | $\theta_f$ | $P_F$ | $f_\delta^{(n)}$ | $\theta_f$ | $a$ | $b$ |
| 0.2 | 0.0841 | 1.3157 | 1746.08 | 0.0925 | 0.9748 | 1930.30 | 0.0554 |
| 0.4 | 0.1681 | 1.8432 | 834.41 | 0.1850 | 1.3081 | 980.76 | 0.1022 |
| 0.6 | 0.2521 | 2.5225 | 348.89 | 0.2775 | 1.6847 | 422.42 | 0.1341 |
| 0.8 | 0.3362 | 3.8195 | 106.37 | 0.3700 | 2.4407 | 105.81 | 0.1261 |
| 1.0 | 0.4202 | 7.7580 | 19.24 | 0.4625 | 7.7580 | 9.97 | 0.0425 |

and (30)) and avoid jumping at truncated scattering angle (Eq. (31)) although the parameter $b$ was quite small in Table 1.

### 2.4. Multiple-scaling method for optically thin regions

Due to rare scatterings occurring in optically thin regions, the noise of the radiance estimated by local estimate method may hide the true radiance field characterization, such as enhanced clear sky radiances near clouds or smoothed radiances in optically thin medium, which greatly depend on contribution of high order of scattering [1,5]. Therefore the higher the scattering order is, the more collision probability should be added to estimate radiance in optically thin regions. Iwabuchi [11] pointed out that similarity relations [24] could be used to scale extinction coefficient for an arbitrary scattering order with different delta fraction when presenting collision-forcing method for optically thin media. However there were no rigorous proofs for this conclusion. So, in this section, we firstly formulate a multiple-scaling method to prove it and then propose a method of gradually increasing sampling probability with scattering order only in optically thin regions.

First adding Eq. (7) and the equality

$$\frac{\omega f_\delta^{(n)}}{(1-f_\delta^{(n)})}\hat{f}(s)\hat{F}_{n-1}(s,\mathbf{\Omega}) = \frac{1}{4\pi}\int_{\mathbf{\Omega}} d\mathbf{\Omega}' \frac{\omega f_\delta^{(n)}}{(1-f_\delta^{(n)})}\delta(\mathbf{\Omega}'-\mathbf{\Omega})\hat{f}(s)\hat{F}_{n-1}(s,\mathbf{\Omega}'), \tag{36}$$

we can obtain

$$\hat{F}_n(s,\mathbf{\Omega}) = -\frac{\omega f_\delta^{(n)}}{(1-f_\delta^{(n)})}\hat{f}(s)\hat{F}_{n-1}(s,\mathbf{\Omega}) + \frac{1}{4\pi}\int_{\mathbf{\Omega}} d\mathbf{\Omega}' \frac{\omega}{(1-f_\delta^{(n)})}P_n^*(\mathbf{\Omega}'\cdot\mathbf{\Omega})\hat{f}(s)\hat{F}_{n-1}(s,\mathbf{\Omega}'), \quad n>0 \tag{37}$$

where $P_n^*(\mathbf{\Omega}'\cdot\mathbf{\Omega})$ is defined as

$$P_n^*(\mathbf{\Omega}'\cdot\mathbf{\Omega}) = f_\delta^{(n)}\delta(\mathbf{\Omega}'-\mathbf{\Omega}) + (1-f_\delta^{(n)})P(\mathbf{\Omega}'\cdot\mathbf{\Omega}). \tag{38}$$

Then by summing up of Eqs. (9) and (37) for all scattering orders, we can obtain

$$\sum_{n=0}^{\infty}\hat{F}_n(s,\mathbf{\Omega}) = -\sum_{n=1}^{\infty}\left[\frac{\omega f_\delta^{(n)}}{(1-f_\delta^{(n)})}\hat{f}(s)\hat{F}_{n-1}(s,\mathbf{\Omega})\right] + \hat{f}(s) + \sum_{n=1}^{\infty}\left[\frac{1}{4\pi}\int_{\mathbf{\Omega}} d\mathbf{\Omega}' \frac{\omega}{(1-f_\delta^{(n)})}P_n^*(\mathbf{\Omega}'\cdot\mathbf{\Omega})\hat{f}(s)\hat{F}_{n-1}(s,\mathbf{\Omega}')\right]. \tag{39}$$

By rearranging Eq. (39), we obtain

$$\sum_{n=0}^{\infty}\hat{F}_n(s,\mathbf{\Omega}) = -\sum_{n=0}^{\infty}\left[\frac{\omega f_\delta^{(n+1)}}{(1-f_\delta^{(n+1)})}\hat{f}(s)\hat{F}_n(s,\mathbf{\Omega})\right] + \hat{f}(s) + \sum_{n=1}^{\infty}\left[\frac{1}{4\pi}\int_{\mathbf{\Omega}} d\mathbf{\Omega}' \frac{\omega}{(1-f_\delta^{(n)})}P_n^*(\mathbf{\Omega}'\cdot\mathbf{\Omega})\hat{f}(s)\hat{F}_{n-1}(s,\mathbf{\Omega}')\right]. \tag{40}$$

Thus the following equations can be given:

$$\hat{F}_n(s,\mathbf{\Omega}) = \begin{cases} \dfrac{1}{4\pi}\displaystyle\int_{\mathbf{\Omega}} d\mathbf{\Omega}' \frac{\omega\hat{f}(s)P_n^*(\mathbf{\Omega}'\cdot\mathbf{\Omega})\hat{F}_{n-1}(s,\mathbf{\Omega}')}{(1-f_\delta^{(n)})\left(1+\dfrac{\omega f_\delta^{(n+1)}\hat{f}(s)}{(1-f_\delta^{(n+1)})}\right)} & n>0 \\ \dfrac{\hat{f}(s)}{\left(1+\dfrac{\omega f_\delta^{(n+1)}\hat{f}(s)}{(1-f_\delta^{(n+1)})}\right)} & n=0 \end{cases}. \tag{41}$$

Now taking the same procedures to Eq. (41) as Eq. (14) in Section 2.2, we have formulas of the solution same as multiple-scaling method for anisotropic phase function except formulas of the new scaled optical quantities for $n$th order of scattering, which is given as

$$\sigma_{n+1}^* = \sigma\left(1+\omega\frac{f_\delta^{(n+1)}}{1-f_\delta^{(n+1)}}\right), \tag{42}$$

$$\omega_n^* = \frac{\omega}{1-(1-\omega)f_\delta^{(n)}}. \tag{43}$$

Eqs. (42) and (43) satisfy similarity relations [11,24] for each order of scattering. The sample's trajectories could be easily simulated with scaled optical quantities in Eqs. (38), (42) and (43). Here it should be noted that the radiance $I_n(\mathbf{r},\mathbf{\Omega})$ for $n$th order does not change although collision density is scaled as Eq. (17) and the scattering points simulated by scaled quantities have $(1-f_\delta^{(n)})$ possibility to be true scattering. Thus local estimate method could be used to estimate radiance at each order of scattering with weight factor of $(1-f_\delta^{(n)})$, we can obtain

$$\Psi_n^*(\mathbf{r},\mathbf{\Omega}) = (1-f_\delta^{(n)})w_n^*\frac{P(\mathbf{\Omega}\cdot\mathbf{\Omega}^*)}{4\pi}\frac{\exp(-\sigma\|\mathbf{r}^*-\mathbf{r}\|)}{\|\mathbf{r}^*-\mathbf{r}\|^2}\delta_{\mathbf{r}^*,\mathbf{\Omega}^*}(\mathbf{r},\mathbf{\Omega}). \tag{44}$$

Above method should be only used in the regions where scattering extinction is below a prescribed parameter $\sigma_s^{(\min)}$ to avoid increasing extra collision chances in optically thick regions. $f_\delta^{(n+1)}$ for $(n+1)$th order could be also determined by sample's directionality parameter $\chi_n$ as

$$f_\delta^{(n+1)} = (f_{\max}-f_{\min})H(\chi_n)+f_{\min}, \tag{45}$$

where the tuning parameter $f_{\max}$ ($f_{\min}$) is maximum (minimum) possibility of virtual scattering. Thus a relatively large value of $f_\delta$ could be used for the transfer of near-isotropic light in optically thin regions to capture the diffusion characterization rapidly.

Although the above methods are derived under the assumption of homogenous medium, these methods could be applied to inhomogeneous medium. In this paper, the simulation procedures are omitted because lots of papers have presented it in detail, such as [11,25–27].

## 3. Validation and evaluations

The forward Monte Carlo simulations have been performed for examining the impacts of multiple-scaling

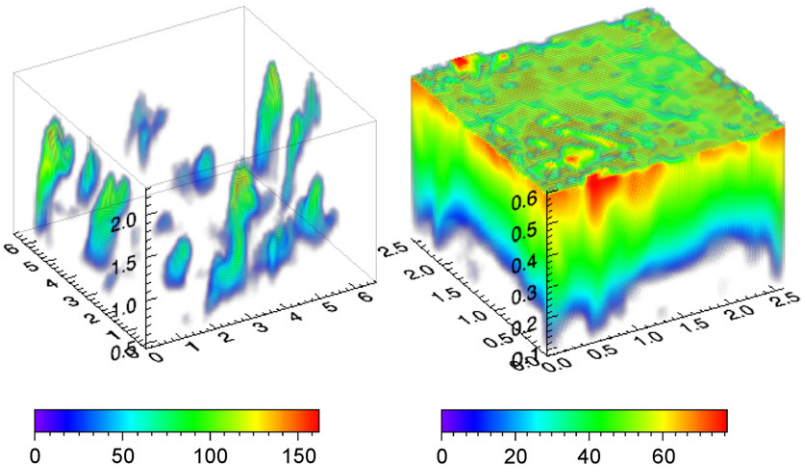


**Fig. 2.** 3D illustration of (left) cumulus and (right) stratocumulus fields, produced by large eddy simulations [28]. The color plates show the cross section of extinction coefficients (in $km^{-1}$). (For interpretation of the references to color in this figure legend, the reader is referred to the web version of this article.)

**Table 2**
Summary of several parameter sets for both multiple-scaling methods.

| Method (abbreviation) | Case | Parameter set |
|---|---|---|
| Multiple-scaling method for anisotropic phase function (MSAPF), using flat and quadratic function for truncation approximations (FTA and QTA) | (1) | $P_{max}=1000$ |
| | (2) | $P_{max}=100$ |
| | (3) | $P_{max}=10$ |
| Multiple-scaling method for optically thin regions (MSOTR) | (1) | $f_{min}=0.0, f_{max}=0.7$ |
| | (2) | $f_{min}=0.5, f_{max}=0.7$ |
| | (3) | $f_{min}=0.7, f_{max}=0.7$ |

methods (MSM) on radiance calculations with respect to standard methods (SM) without optimizations. We selected several plane-parallel atmosphere (PPA) cases and two 3D cloud cases to validate MSM and evaluate numerical efficiency of MSM for typical cloudy atmospheres.

### 3.1. Setup of numerical experiments

MSM for optically thin regions (MSOTR) is no biased method, so simulations for PPA cases were performed for examining biases due to MSM for anisotropic phase function (MSAPF) only. The phase function shown in Fig. 1 was used for validating MSAPF. The surface was assumed to a flat, lambertian reflector with albedo of 0.05. Simulations were also done for both 3D cloud fields to evaluate numerical efficiency of both MSM. Both fields were taken from large-eddy simulations described in [28], illustrated in Fig. 2. One was a cumulus field over land, having an extension of 6.6 km × 6.6 km with a horizontal resolution of 100 m, vertical depth of 1.44 km with a vertical resolution of 40 m, filled with some scattered clouds; the second one was a maritime stratocumulus, an extension of 2.6 km × 2.6 km with 50 m resolution, depth of 0.45 km with 10 m resolution. Both fields were water clouds, composed of water droplets with a constant droplet number (100 $cm^{-3}$ for the cumulus and 70 $cm^{-3}$ for the

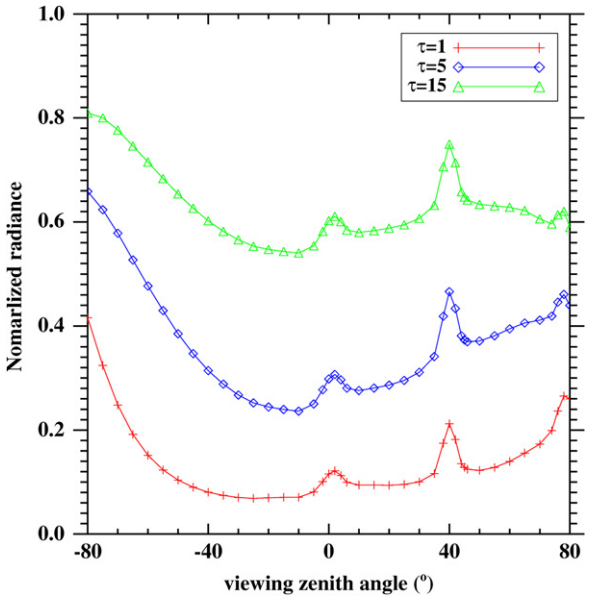


**Fig. 3.** Reflected radiances for solar zenith angle 40° in plane-parallel clouds as functions of viewing zenith angles along the principal plane, which were used as benchmark values to validate the results calculated by multiple-scaling method for anisotropic phase function (MSAPF). The negative (positive) viewing zenith angles correspond to forward (backward) viewing directions.

stratocumulus), which was assumed to calculate effective radii for each cloud grid box. The cloud optical properties at the wavelength of 670 nm (extinction coefficients, single scattering albedo, and scattering phase function) were calculated using Mie theory for gamma size distributions with the assumption of effective variance of 0.1. The domain average cloud optical thickness (COD) was 3.23 for cumulus and 14.03 for stratocumulus. Aerosols were included in two scenes. The rural and maritime types of aerosols were chosen for cumulus with aerosol optical thickness (AOD) of 0.138 and stratocumulus fields with AOD of 0.045 [29]. A standard US atmosphere was used to

consider the Rayleigh scattering [29]. The surface was assumed to be a flat, lambertian reflector with albedo of 0.2 for cumulus and 0.05 for stratocumulus.

In this paper, radiances were normalized and defined as

$$\rho = \pi I/(F_0 \cos\theta_0), \tag{46}$$

where $I$ is radiance, $F_0$ is incident solar irradiance, and $\theta_0$ is the solar zenith angle. Bias errors were introduced to check biases due to MSM, defined as

$$\Delta\rho_{MSM} = \left(\frac{\rho_{MSM}-\rho_{SM}}{\rho_{SM}}\right) \times 100\%. \tag{47}$$

In addition, efficiency factors were used to evaluate the numerical efficiency, defined as

$$\eta_{MSM} = \frac{\delta_{SM}^2 T_{SM}}{\delta_{MSM}^2 T_{MSM}}, \tag{48}$$

where $\delta$ is root-mean-square relative error (RMSE), $T$ is single-CPU time with 2.5 GHz. The subscript in Eqs. (47) and (48) means specific method was used. True RMSE could be approximately estimated as RMSE of a set of samples' batches [9]. This way could underestimate true RMSE [8]. But its accuracy would be enough especially for larger RMSE. It should be noted that some parameters remained unchanged during simulations. For both *MSM*, $h_{\max}=5$, $\chi_{\max}=0.9$ and $\chi_{\min}=0.4$ (see the definitions in [11]); for MSOTR, $\sigma_s^{(\min)}=5\,\mathrm{km}^{-1}$. For more detailed parameters see Table 2.

### 3.2. Biases due to multiple-scaling method

Reflected radiances along the principal plane shown in Fig. 3 were calculated for PPA cases with optical thickness $\tau=1$, 5, and 15 using a large number of samples ($2\times10^9$ for $\tau=1$; $1\times10^9$ for others). The Monte Carlo noise was less than 0.13%. Results computed without optimizations shown in Fig. 3 were considered as benchmark values. The bias errors for results computed with MSAPF are shown in Fig. 4, using flat and quadratic function for truncation approximations (FTA and QTA), with the tuning parameter $P_{\max}=10$, 100, and 1000. In addition, Table 3 summarizes the mean and maximum bias errors for these results.

The bias errors were extremely small (always less than 0.54%) in all viewing directions for both TA with various $P_{\max}$. When $P_{\max}$ was small, the delta fraction was large.

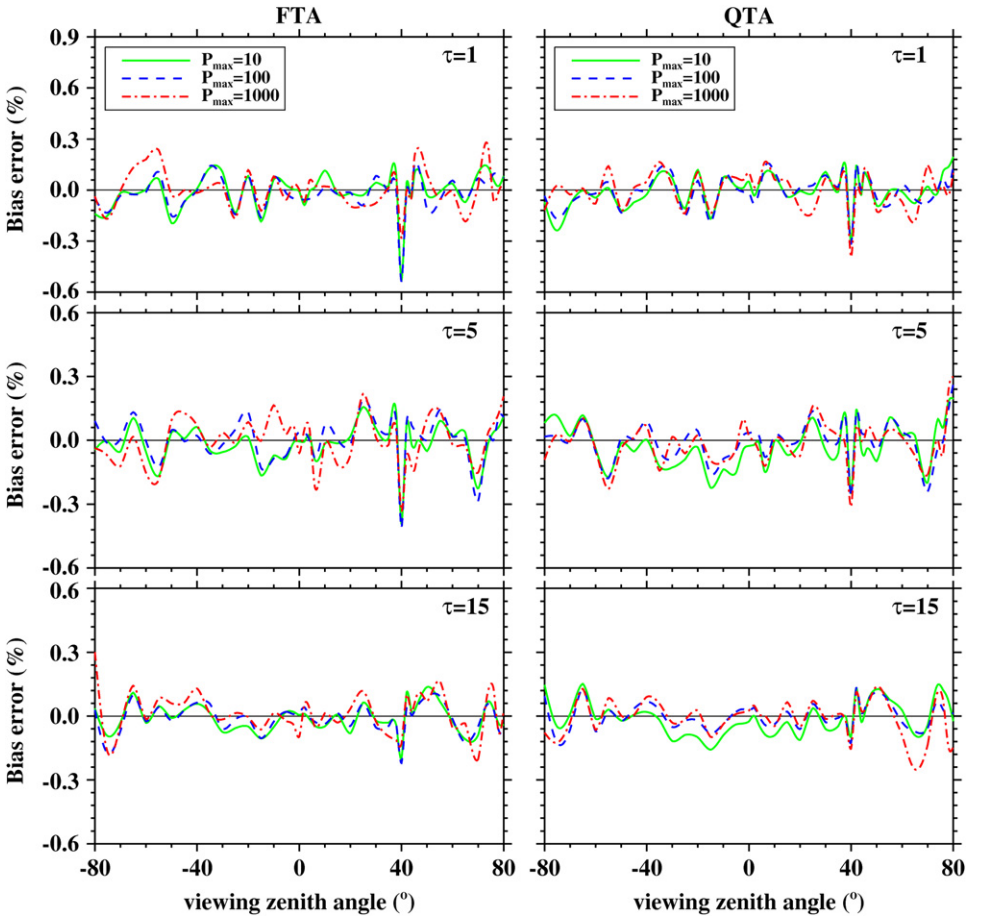


**Fig. 4.** Bias errors of reflected radiance as functions of viewing zenith angles, calculated by MSAPF with various tuning parameters $P_{\max}=10$, 100, and 1000 and with (left) flat function and (right) quadratic function for truncation approximations (FTA and QTA). Negative (positive) viewing zenith angles are explained in Fig. 3.

**Table 3**
Bias and standard errors of reflected radiance for plane-parallel clouds using MSAPF with different cases (see Table 2).

| $\tau$ | MSAPF | Maximum bias (%) | | Mean bias (%) | | Mean std error (%) | |
|---|---|---|---|---|---|---|---|
| | Case | FTA | QTA | FTA | QTA | FTA | QTA |
| 1.0 | (1) | 0.2837 | 0.3942 | 0.0808 | 0.0848 | 0.0726 | 0.0577 |
| | (2) | 0.5384 | 0.3189 | 0.0783 | 0.0737 | 0.0469 | 0.0373 |
| | (3) | 0.5315 | 0.3082 | 0.0769 | 0.0779 | 0.0317 | 0.0312 |
| 5.0 | (1) | 0.3343 | 0.3133 | 0.0909 | 0.0739 | 0.0666 | 0.0506 |
| | (2) | 0.4137 | 0.2680 | 0.0714 | 0.0672 | 0.0378 | 0.0271 |
| | (3) | 0.3949 | 0.2514 | 0.0646 | 0.0875 | 0.0226 | 0.0219 |
| 15.0 | (1) | 0.3003 | 0.2501 | 0.0749 | 0.0656 | 0.0517 | 0.0381 |
| | (2) | 0.2205 | 0.1317 | 0.0518 | 0.0495 | 0.0274 | 0.0179 |
| | (3) | 0.2000 | 0.1580 | 0.0529 | 0.0634 | 0.0147 | 0.0141 |

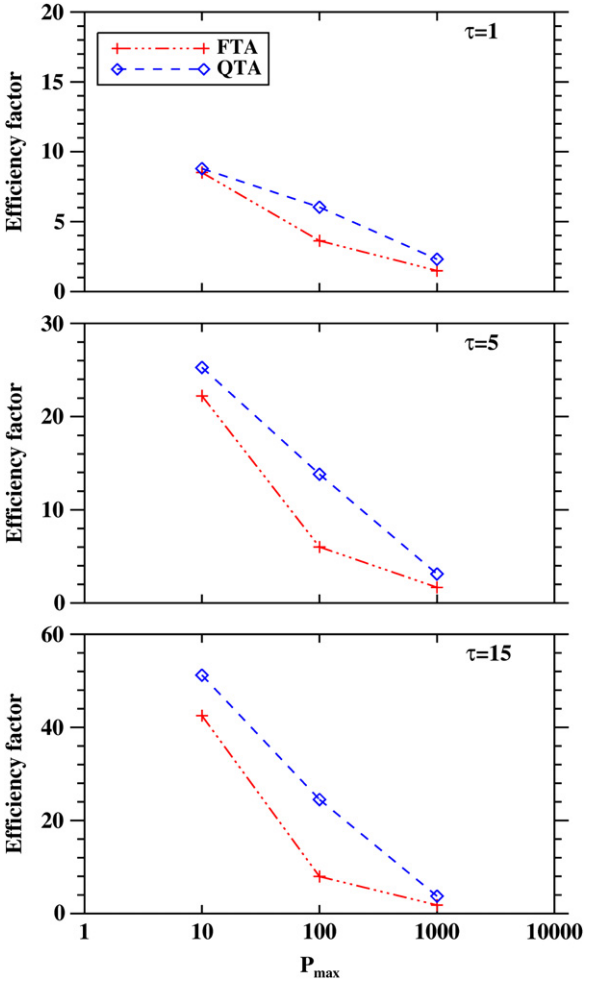


**Fig. 5.** Efficiency factors of reflected radiance using FTA and QTA (see Table 2) as functions of the tuning parameters $P_{max}$.

Therefore smaller $P_{max}$ would cause larger bias. But Table 3 shows that smaller $P_{max}$ reduced mean bias errors more largely for almost cases. The main reason was that bias errors were covered by simulations noises especially for larger $P_{max}$ although the noises were very small. In some sense, it means that MSAPF was highly accurate for reflected radiance calculation even with the smallest tuning parameter $P_{max}$. In addition, the mean bias error for QTA was slightly larger than that of FTA when $P_{max} = 10$, which was due to larger delta fraction for QTA than for FTA (see Fig. 1). But Fig. 4 depicts that

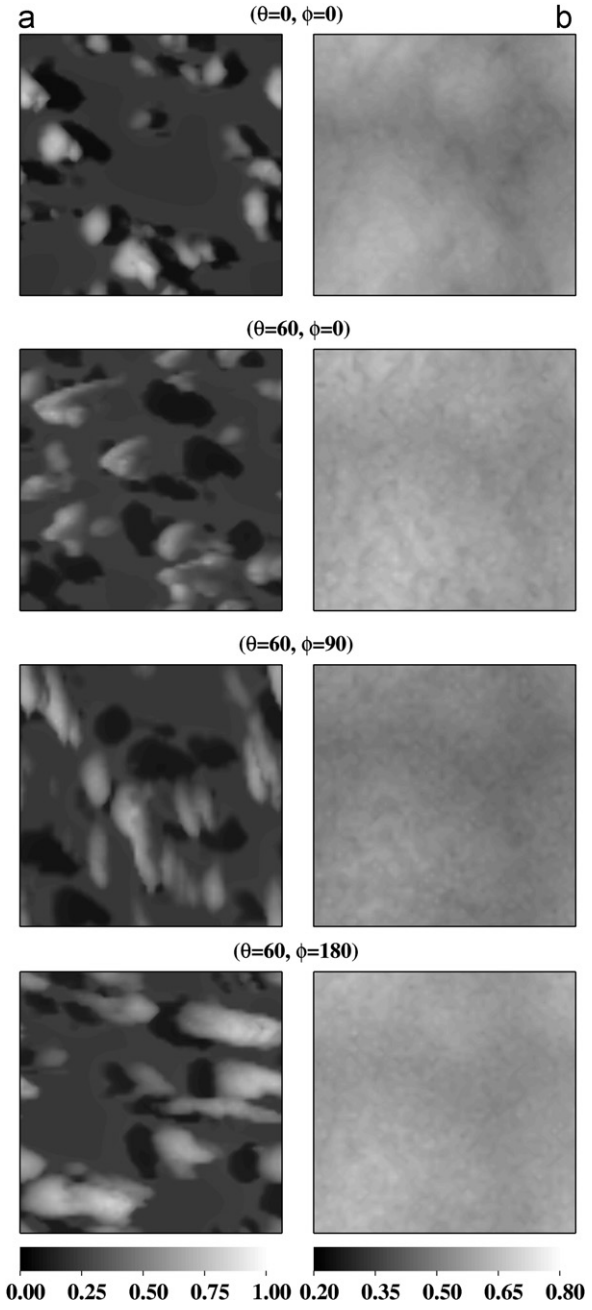


**Fig. 6.** Radiance fields reflected from top of (a) cumulus and (b) stratocumulus fields in four directions from (top) to (bottom), which were used as benchmark values to validate the results calculated by multiple-scaling methods for anisotropic phase function and optically thin regions (MSAPF and MSOTR).

slightly larger bias error for FTA was occurred in glory direction ($\theta=40^\circ$) especially in the optically thin case ($\tau \leq 5$). The reason was that less similarity between truncated phase function and original one may cause large contribution bias for low-order scattering (see Fig. 1) where the contribution for low-order scattering dominated. In the optically thick case ($\tau=15$), both TA exhibited very little bias even for glory direction where high-order scattering dominated. In general, we could find that QTA was slightly more accurate than FTA for almost cases when comparing maximum bias errors. Finally, efficiency factors are also shown in Fig. 5. The results show that efficiency factor increased as $P_{\max}$ decreased and $\tau$ increased for both TA. It has been increased by a factor of 42 for FTA and 51 for QTA when $\tau=15$. QTA was more efficient than FTA for all cases especially when $P_{\max}=100$. In general, we could find that QTA could have more accuracy in glory direction and almost same accuracy in others as well as higher numerical efficiency.

### 3.3. Numerical efficiency for multiple-scaling methods

Several simulation schemes for both 3D cloud fields were performed with the sun in the direction $(\theta_0,\phi_0)=(30^\circ,180^\circ)$. Radiances were computed at four angles, corresponding to the viewing angles of experiments for Phase 2 cloud fields of I3RC [30], that was, at $(\theta,\phi)=(0^\circ,0^\circ)$, $(60^\circ,0^\circ)$, $(60^\circ,90^\circ)$, and $(60^\circ,180^\circ)$. Radiances for each scheme using $N_{col}=(10^3,10^4,10^5)$ samples per pixel for cumulus

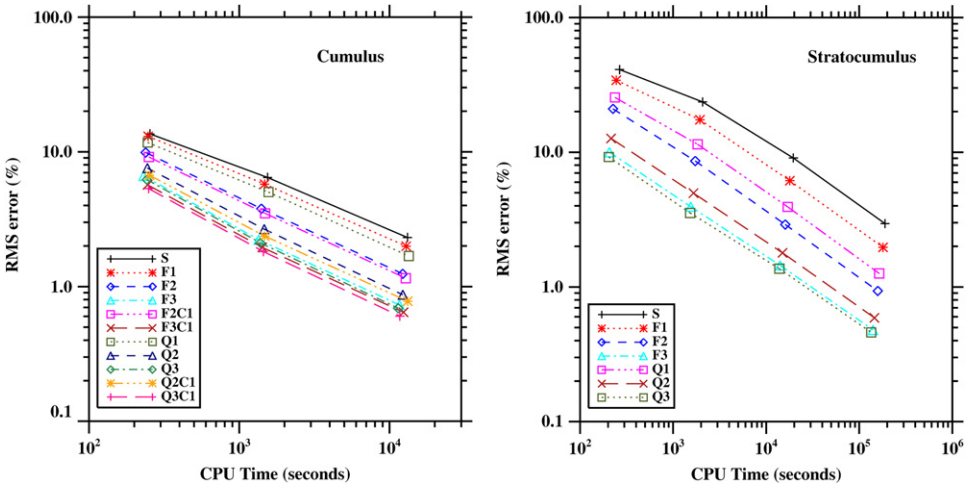


**Fig. 7.** RMSE of reflected radiance for (left) cumulus and (right) stratocumulus fields as functions of single-CPU computation time for multiple-scaling methods with different parameter sets in Table 2. RMSE were evaluated with benchmark values and then averaged over all pixels and viewing directions. For each legend, a few symbols are combined to represent each simulation schemes, where we denote S as standard simulation without optimizations, Q (F) as QTA (FTA) for MSAPF, C as MSOTR, and Arabic numbers as parameter sets of each method shown in Table 2. For example, Q3C1 indicates that simulations were performed using both MSAPF with case (3) and QTA and MSOTR with case (1) (see more details in Table 2).

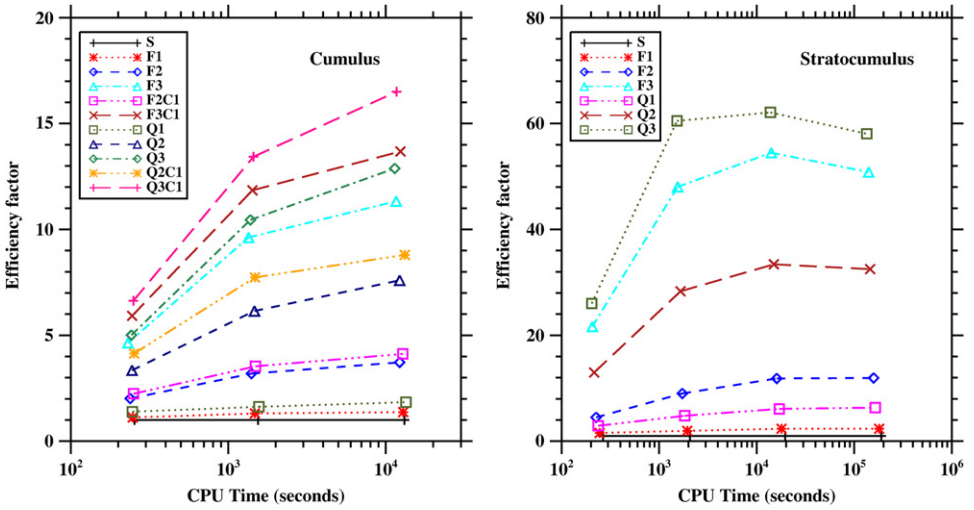


**Fig. 8.** Efficiency factors of reflected radiance for (left) cumulus and (right) stratocumulus fields, evaluated with benchmark calculations and then averaged over all pixels and viewing directions, as functions of single-CPU computation time for multiple-scaling methods with various parameter sets. The interpretation of legend is same as Fig. 7.

and $N_{col}=(10^3,10^4,10^5,10^6)$ samples per pixel for stratocumulus were compared with benchmark values using $10^{10}$ samples totally. Fig. 6 illustrates radiance fields in each direction for both cloud fields.

Although MSAPF is the biased method, it is highly accurate (In Table 3, maximum bias error less than 0.5%; mean bias error less than 0.1%). It means that the bias error due to MSAPF could be negligible when accuracy of 1% was expected. Thus the most important issue is numerical efficiency for various schemes. RMSE as functions of single-CPU time are shown in Fig. 7, which were gradually reduced for both cloud fields as $P_{\max}$ decreased. For example, the RMSE were reduced to 0.69% for cumulus with $10^5$ samples per pixel and 0.46% for stratocumulus with $10^6$ samples per pixel, when Q3 scheme (see description in Fig. 7) was performed and the corresponding efficiency factors were increased to 12.88 and 58.06, respectively, in Fig. 8. At same time, it demonstrates that MSAPF was highly efficient especially for stratocumulus field with a large domain average optical thickness. In addition, QTA was more efficient than FTA especially when $P_{\max}=100$, where the efficiency factors for stratocumulus were 11.86 for FTA and 33.41 for QTA when $10^5$ samples per pixel was used. This was due to more truncation fraction for high-order scattering when QTA was used (see Fig. 1). In general, MSAPF with QTA is more efficient in computing reflected radiance.

**Table 4**
RMSE, Bias errors and simulation time of reflected radiance for cumulus field using MSOTR with three cases and MSAPF with case (3) (see Table 2). The $10^6$ samples per pixel were used.

| MSOTR case | RMSE (%) | Bias (%) | Time (s) |
|---|---|---|---|
| (1) | 0.6020 | 0.6650 | 12248.8 |
| (2) | 0.5850 | 0.7814 | 12657.6 |
| (3) | 0.5804 | 1.0149 | 12838.5 |

With careful examination, we can know that efficiency factor for cumulus was much small. This was due to less collision chances in optically thin regions for cumulus. MSOTR has been applied to solve this problem. RMSE for Q3C1 scheme with $10^5$ samples per pixel was reduced from 0.69% to 0.60%, and the corresponding efficiency factor was increased from 12.88 to 16.50 while the simulation timing nearly was not increased. MSOTR increased collision chance for optically thin regions adaptively. The higher efficiency could be accomplished when QTA coupled with MSOTR. In order to further show the ability of MSOTR, bias errors instead of the RMSE were calculated for three simulation cases. Because true RMSE were close to bias errors as the underestimated RMSE were less than bias errors. We could find that bias errors and simulation timing increased as $f_{\min}$ increased in Table 4. It shows that gradually increasing scattering extinction coefficients with scattering order could have higher numerical efficiency.

RMSE for each viewing direction were different (see Fig. 9). We could find that large RMSE occurred in backward viewing direction. Illuminations from cloud sides were main 3D effects in this direction where contribution of low-order scattering was large. In other words, MSAPF could not reduce noises caused by low-order scattering rapidly although it could handle high-order scattering efficiently. This is limitation of MSAPF. The problem may be solved by detector directional importance sample [8].

## 4. Summary and conclusions

We have formulated two multiple-scaling methods for convergence acceleration of radiance estimates for Monte Carlo radiative transfer model in cloudy atmosphere. Both methods were derived from integral radiative transfer equation rigorously and could be used to construct Monte Carlo simulation procedures and formulate local estimate

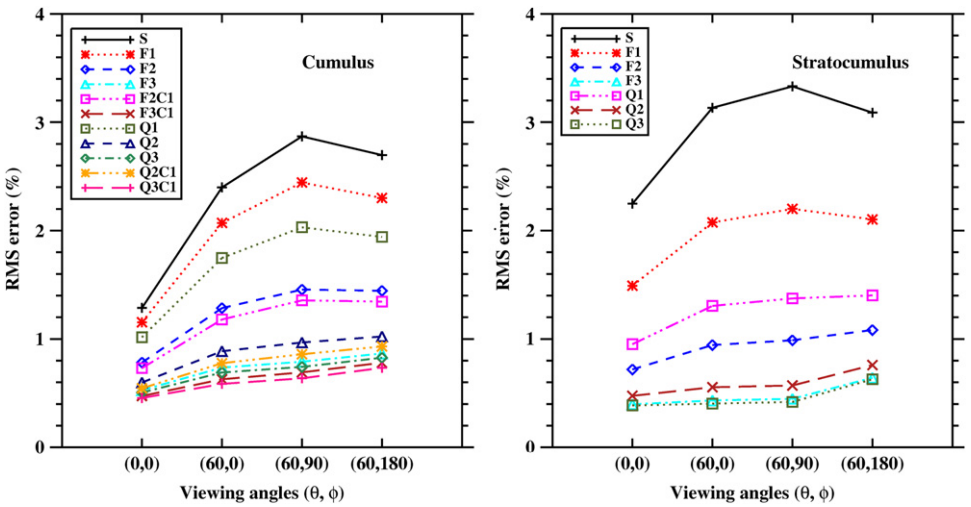


**Fig. 9.** RMSE of reflected radiance for (left) cumulus field with $10^5$ samples per pixel and (right) stratocumulus field with $10^6$ samples per pixel, evaluated with benchmark calculations and averaged over all pixels, as functions of viewing angles for multiple-scaling methods with various parameter sets. The interpretation of legend is same as Fig. 7 too.

method directly. The core of both methods is to simulate sample's trajectories in the variable medium (i.e., the optical properties of the medium could be modified adaptively according to sample's statistical directionality parameter). For the first one, we approximate phase function as a linear mixture of delta function and truncated phase function and increase truncation fraction with decreasing sample's statistical directionality parameter. More importantly, we introduce quadratic functions rather than flat functions to replace sharp forward peaks of phase function, which can take more truncation fraction to reduce computation burden significantly and maintain continuity at truncated angles to improve accuracy slightly, especially in glory direction. Moreover, a single prescribed parameter as a value of phase function is used to determine maximum truncation fraction for each phase function, which is suitable for solving three-dimensionally inhomogeneous atmosphere. For the second method, we firstly proofed that similarity relations could be used for each order of scattering under rigorous derivation. Then through increasing collision possibility (i.e., scattering extinction coefficient) only in optically thin regions with decreasing sample's statistical directionality parameter, we could rapidly reduce radiance's noise nearly without extra time. Furthermore, we could combine both methods to bring higher numerical efficiency for partly cloudy atmosphere, such as cumulus. It is very useful to examine three-dimensional interaction between clear sky and clouds, such as enhancement of clear sky near clouds.

Generally, due to large truncation fraction and collision possibility for high order of scattering (i.e., small sample's statistical directionality parameter), both methods can rapidly reduce radiance's noise caused by high-order scattering. In other words, the main advantage of both methods is that they are quite efficient to solve Monte Carlo radiative transfer in partly cloudy atmosphere with large domain optical thickness.

## Acknowledgements

The authors thank Victor Venema from Meteorological Institute of Bonn University for the high-resolution cloud fields and are grateful to two anonymous reviewers for their useful comments to improve the manuscript.

## References

[1] Marshak A, Davis A, Wiscombe W, Cahalan R. Radiative smoothing in fractal clouds. J Geophys Res 1995;100(D12):26247–61.
[2] Iwabuchi H, Hayasaka T. Effects of cloud horizontal inhomogeneity on the optical thickness retrieved from moderate-resolution satellite data. J Atmos Sci 2002;59:2227–42.
[3] Várnai T, Marshak A. A method for analyzing how various parts of clouds influence each other's brightness. J Geophys Res 2003;108:4706.
[4] Kobayashi T, Masuda K, Sasaki M, Mueller J. Monte Carlo simulations of enhanced visible radiance in clear-air satellite fields of view near clouds. J Geophys Res 2000;105:26569.
[5] Nikolaeva OV, Bass LP, Germogenova TA, Kokhanovsky AA, Kuznetsov VS, Mayer B. The influence of neighbouring clouds on the clear sky reflectance studied with the 3-D transport code RADUGA. J Quant Spectrosc Radiat Transfer 2005;94:405–24.
[6] Várnai T, Marshak A. MODIS observations of enhanced clear sky reflectance near clouds. Geophys Res Lett 2009;36:L06807.
[7] Wen G, Marshak A, Cahalan R, Remer L, Kleidman R. 3-D aerosol-cloud radiative interaction observed in collocated MODIS and ASTER images of cumulus cloud fields. J Geophys Res 2007;112:D13204.
[8] Buras R, Mayer B. Efficient unbiased variance reduction techniques for Monte Carlo simulations of radiative transfer in cloudy atmospheres: the solution. J Quant Spectrosc Radiat Transfer 2011;112:434–47.
[9] Pincus R, Evans K. Computational cost and accuracy in calculating three-dimensional radiative transfer: results for new implementations of Monte Carlo and SHDOM. J Atmos Sci 2009;66:3131–46.
[10] Iwabuchi H, Suzuki T. Fast and accurate radiance calculations using truncation approximation for anisotropic scattering phase functions. J Quant Spectrosc Radiat Transfer 2009;110:1926–39.
[11] Iwabuchi H. Efficient Monte Carlo methods for radiative transfer modeling. J Atmos Sci 2006;63:2324–39.
[12] Barker H, Goldstein R, Stevens D. Monte Carlo simulation of solar reflectances for cloudy atmospheres. J Atmos Sci 2003;60:1881–94.
[13] McKellar BHJ, Box MA. The scaling group of the radiative transfer equation. J Atmos Sci 1981;38:1063–8.
[14] Modest M. Radiative heat transfer: Academic Pr; 2003.
[15] Nakajima T, Tanaka M. Algorithms for radiative intensity calculations in moderately thick atmospheres using a truncation approximation. J Quant Spectrosc Radiat Transfer 1988;40:51–69.
[16] Wiscombe W. The delta-M method: rapid yet accurate radiative flux calculations for strongly asymmetric phase functions. J Atmos Sci. 1977;34:1408C22.
[17] Antyufeev V. Monte Carlo method for solving inverse problems of radiation transfer. Walter de Gruyter; 2000.
[18] Suzuki T, Nakajima T, Tanaka M. Scaling algorithms for the calculation of solar radiative fluxes. J Quant Spectrosc Radiat Transfer 2007;107:458–69.
[19] Cahalan RF, Oreopoulos L, Wen G, Marshak A, Tsay SC, DeFelice T. Cloud characterization and clear-sky correction from Landsat-7. Remote Sens Environ 2001;78:83–98.
[20] Evans K, Marshak A. Numerical Methods.3D Radiative Transfer in Cloudy Atmospheres. New York: Springer; 2005 p. 243–281.
[21] Marchuk G, Mikhailov G, Nazaraliev M. The Monte Carlo methods in atmospheric optics. New York: Springer; 1980.
[22] Davis A, Knyazikhin Y. A primer in 3D radiative transfer. 3D Radiative Transfer in Cloudy Atmospheres. New York: Springer; 2005 p. 153–242.
[23] Davis A. Effective propagation kernels in structured media with broad spatial correlations, Illustration with large-scale transport of solar photons through cloudy atmospheres. Comput Methods Transport 2006:85–140.
[24] Liou K. An introduction to atmospheric radiation: Academic Pr; 2002.
[25] Cornet C, C-Labonnote L, Szczap F. Three-dimensional polarized Monte Carlo atmospheric radiative transfer model (3DMCPOL): 3D effects on polarized visible reflectances of a cirrus cloud. J Quant Spectrosc Radiat Transfer 2010;111:174–86.
[26] Mayer B. I3RC phase 1 results from the MYSTIC Monte Carlo model. Extended abstract for the I3RC (Intercomparison of 3D radiation codes) workshop. Tucson, Arizona 1999.
[27] Mayer B. Radiative transfer in the cloudy atmosphere. Eur Phys J Conf 2009;1:75–99.
[28] Venema V, Meyer S, García S, Kniffka A, Simmer C, Crewell S, et al. Surrogate cloud fields generated with the Iterative Amplitude Adapted Fourier Transform algorithm. Tellus A. 2006;58:104–20.
[29] Kneizys F, Shettle E, Abreu L, Chetwynd J, Anderson G, Gallery W, et al. Users guide to LOWTRAN 7;1988.
[30] Cahalan R, Oreopoulos L, Marshak A, Evans K, Davis A, Pincus R, et al. The International Intercomparison of 3D Radiation Codes (I3RC): Bringing together the most advanced radiative transfer tools for cloudy atmospheres. Bull Am Meteor Soc 2005;86:1275 C93.